SLAC-PUB-12901
October 2007

Proton Form Factors measurements in the time-like region

F Anulli, *from the BABAR Collaboration*
Laboratori Nazionali di Frascati dell'INFN, via E. Fermi 40, I-00044 Frascati (RM), Italy
E-mail: fabio.anulli@lnf.infn.it

Abstract. I present an overview of the measurement of the proton form factors in the time-like region. *BABAR* has recently measured with great accuracy the $e^+e^- \to p\bar{p}$ reaction from production threshold up to an energy of ~ 4.5 GeV, finding evidence for a ratio of the electric to magnetic form factor greater than unity, contrary to expectation. In agreement with previous measurements, *BABAR* confirmed the steep rise of the magnetic form factor close to the $p\bar{p}$ mass threshold, suggesting the possible presence of an under-threshold $N\bar{N}$ vector state. These and other open questions related to the nucleon form factors both in the time-like and space-like region, wait for more data with different experimental techniques to be possibly solved.

1. Introduction

The nucleon form factors are among the very first topics studied in subnuclear physics. However, in spite of several decades of experimental investigation, the structure and the nature of the nucleons have not yet been fully revealed, as confirmed by the rather unexpected results recently obtained. The form factors are introduced to account for the non point-like structure of the hadrons and play a fundamental role in understanding the hadron dynamics. The vertex operator Γ^μ describing the hadron current in the Feynman diagrams of Fig. 1 and 2, is function of the quadrimomentum transfer, q^2, that is the only Lorentz invariant available:

$$\Gamma^\mu \;=\; F_1(q^2)\,\gamma^\mu \;+\; \frac{ik}{2m_p}\,F_2(q^2)\,\sigma^{\mu\nu}q_\nu. \qquad (1)$$

Here, k is the nucleon magnetic moment, m_p is the proton mass and $F_1(q^2)$ and $F_2(q^2)$ are the Dirac and Pauli form factors. Usually, results are expressed in terms of the electric G_E and magnetic G_M form factors, rather than of F_1 and F_2, defined as:

$$G_E(q^2) \;\equiv\; F_1(q^2) + \frac{kq^2}{4m_p^2}\,F_2(q^2); \qquad G_M(q^2) \;\equiv\; F_1(q^2) + F_2(q^2). \qquad (2)$$

In the nucleon Breit reference frame, where the two nucleons are back-to-back, G_M and G_E enter respectively the spin-flip and non spin-flip amplitude and do not interfere.

The form factors are analytic functions defined for every q^2 value. They are real for $q^2 < 0$, the so-called space-like region, which can be accessed studying the electron-proton elastic scattering shown in Fig. 1, while they are complex for $q^2 > 4m_\pi^2$, that is above the production threshold for hadron final states in e^+e^- annihilations (see Fig. 2). Data can be collected only above

Submitted to Applied Physics Letters

Work supported in part by US Department of Energy contract DE-AC02-76SF00515
SLAC, Stanford University, Stanford, CA 94025

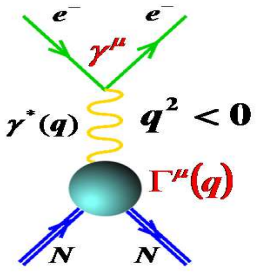

Figure 1. The Feynman diagram of $ep \to ep$ elastic scattering.

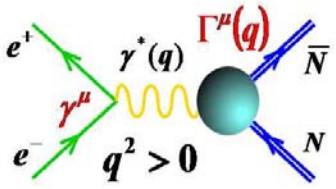

Figure 2. The Feynman diagram of $e^+e^- \to p\bar{p}$ annihilation.

the $p\bar{p}$ production threshold, but the presence of resonances in the unphysical region, that is for $q^2 < 4m_p^2$, can influence the shape of the form factor function in the physical region. The analyticity of the form factor functions allows to calculate their behavior in the unphysical region by means of dispersion relations using the available data in the time-like and space-like regions.

The space-like region has been investigated up to $-q^2 \sim 30\,(\mathrm{GeV}/c)^2$. The measurement of the $|G_E/G_M|$ ratio, recently performed at the Jefferson Laboratory looking at the ratio between transverse and parallel polarization of the outgoing proton, shows a negative slope as a function of $qquadro$, approaching zero at $-q^2 \simeq 8\,(\mathrm{GeV}/c)^2$ [1], contradicting previous results obtained by means of the Rosenbluth method. Although the discrepancy seems to be due to radiative corrections, in particular to two-photon exchange contribution, the question is not yet closed.

In $e^+e^- \to p\bar{p}$ annihilation the q^2 is given by the center-of-mass (CM) energy of the colliding electrons and corresponds to the invariant mass of the final $p\bar{p}$ system, $m_{p\bar{p}}$:

$$q^2 \equiv s \equiv m^2_{p\bar{p}} = (p_{e^-} + p_{e^+})^2 \geq 4m_p^2. \tag{3}$$

The $e^+e^- \to p\bar{p}$ differential cross section is written as a function of G_E and G_M:

$$\frac{d\sigma}{d\Omega}(q^2, \theta_p) = \frac{\alpha^2 \beta C}{4q^2}\left[\left(1 + \cos^2\theta_p\right)\left|G_M(q^2)\right|^2 + \frac{4m_p^2}{q^2}\sin^2\theta_p\left|G_E(q^2)\right|^2\right], \tag{4}$$

where $\beta = \sqrt{1 - 4m_p^2/q^2}$, $C \sim y/(1 - exp(-y))$ and $y = \pi\alpha m_p/(\beta q)$. The Coulomb correction factor C is effective only very near the production threshold, diverging as $1/\beta$ and making the cross section non-zero at threshold [2].

The form factors in the time-like region can be obtained also measuring the $p\bar{p} \to e^+e^-$ annihilation. The cross section differs from that of $e^+e^- \to p\bar{p}$ for the phase space factor, while the dependences on G_E and G_M are the same. Indeed, important results have been obtained using both techniques.

Recently, the $BABAR$ experiment has measured $\sigma(e^+e^- \to p\bar{p})$ with great accuracy and over a wide range of center of mass energies, using a new technique based on the reconstruction of the initial state radiation (ISR) process $e^+e^- \to p\bar{p}\gamma$. The $BABAR$ measurements are described in detail in the following sections and the results are discussed in comparison with the previous measurements, taking also into account the experimental situation in the space-like region and the available data on the neutron time-like form factor. I will conclude summarizing the perspectives in this subject.

2. Measurement of $e^+e^- \to p\bar{p}\gamma$ by $BABAR$

Initial state radiation (ISR) processes can be effectively used to measure e^+e^- annihilation at high luminosity e^+e^- storage rings, such as the B-factory PEP-II [3]. A large mass range is

accessible in a single experiment contrary to the case with fixed energy colliders, which are optimized only in a limited region. In addition, the broad-band coverage may result also in greater control of systematic effects.

BABAR has already published several results on hadron spectroscopy and on measurement of the ratio R $= \sigma(e^+e^- \to \text{hadrons})/\sigma(e^+e^- \to \mu^+\mu^-)$ based on this technique. Among them the measurement of the cross section $\sigma(e^+e^- \to p\bar{p}\gamma)$, described in detail in Ref. [4].

The cross section for $p\bar{p}$ production via ISR is related to the cross section for the direct annihilation $e^+e^- \to p\bar{p}$ through

$$\frac{d\sigma(s,x)}{d\Omega_\gamma dx} = W(s,x,\Omega_\gamma)\ \sigma_{p\bar{p}}(m^2_{p\bar{p}}), \qquad m^2_{p\bar{p}} = s(1-x); \tag{5}$$

where $x = 2E_\gamma/\sqrt{s}$, E_γ and Ω_γ are the energy and angle of the radiated photon in the e^+e^- center of mass frame and $\sqrt{s}$ is the nominal CM energy of the collider. The radiator function $W(s,x,\Omega_\gamma)$ describes the energy spectrum of the virtual photon and can be computed to an accuracy better than 1%. The direction of radiated photon is peaked along the initial beams, but for $\sqrt{s} \simeq 10$ GeV the fraction at large angle is relatively large. We should note also that at this energy the contribution of final state radiation is very small and there is no interference term with ISR, because of the opposite charge parity of the hadron final state.

ISR events are tagged by detecting a photon radiated at an angle $22^\circ < \theta_\gamma < 137^\circ$ in the laboratory frame, with an energy in the CM frame greater than 3 GeV, to get rid of the non ISR multi-hadrons background. The resulting acceptance is of the order of $\sim 15\%$.

This quite large loss of statistics is fully compensated by the fact that the $p\bar{p}$ system is boosted oppositely to the photon direction, that is at wide angle. As a consequence, the reconstruction efficiency is not vanishing at production threshold and there is essentially full angular coverage in the $p\bar{p}$ center of mass frame.

The asymmetric B-factory PEP-II (9 GeV e^- colliding with 3.1 GeV e^+) and the *BABAR* detector are described in detail elsewhere [5]. The information from the tracking system, a 5 layers Silicon Vertex Tracker and a 40 layers Drift Chamber, are used to measure angles and momenta of charged particles. Charged particle identification is obtained combining the information from the Cherenkov detector with measurement of the specific ionization in the tracking system and of the energy deposition in the CsI electromagnetic calorimeter. Muons are identified in the Resistive Plate Counters installed in the magnet yoke of the *BABAR* solenoid, while photons are detected in the calorimeter.

Detailed Montecarlo simulations are performed to determine detector acceptances and efficiencies and to estimate the different background sources. Montecarlo generators for the simulation of the hadron final states are developed according to the approach suggested by the authors of Ref. [6]. Multiple soft-photon emission from initial-state particles are implemented with the structure function technique [7, 8], while final state radiation is simulated by means of the PHOTOS package [9]. The accuracy of the radiative corrections is of the order of 1%.

To get rid of the huge background coming from other ISR processes, like $\pi^+\pi^-\gamma$, $K^+K^-\gamma$ and $\mu^+\mu^-\gamma$, both charged tracks are required to be well identified as proton candidates. A kinematic fit under the different mass hypothesis is then performed, selecting signal according to the fit χ^2.

The most important source of background is the process $e^+e^- \to p\bar{p}\pi^0$, where easily a soft photon is lost or the two photons are merged and not disentangled by the reconstruction code.

The overall detection efficiency is about 18%. Moreover, as it is shown in Fig. 3 and 4, the efficiency is only slightly dependent from both the mass of the $p\bar{p}$ system and the proton emission angle in the $p\bar{p}$ CM frame, $\cos\theta_p$. These features are extremely important to study the form factor behavior in the region close to the production threshold, not reachable by conventional e^+e^- experiments, and to disentangle the electric and magnetic form factor measuring the

angular distributions (see Eq. 4). Both conventional e^+e^- and $p\bar{p}$ experiments, in fact, can not cover the region at small angles because of the beam line instrumentation.

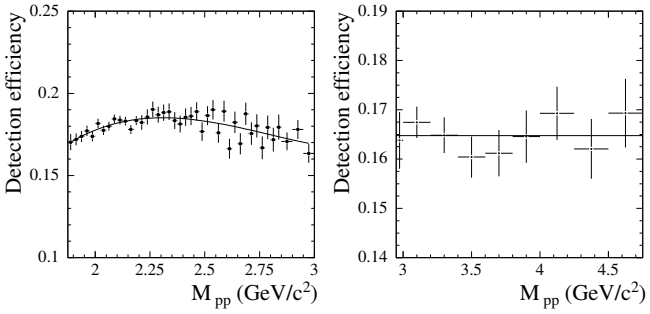

Figure 3. Detection efficiency as a function of the $p\bar{p}$ final state mass. The line on the left plot is the fit to a third-order polinomial. The efficiency for $m_{p\bar{p}}$ is fit to a constant value.

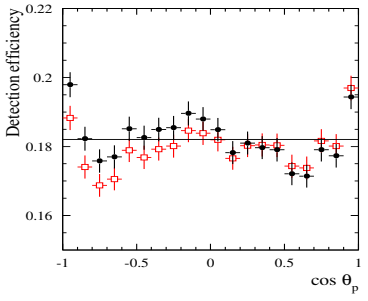

Figure 4. The angular dependence of the detection efficiency in the $p\bar{p}$ CM frame, before (open square) and after (filled circles) corrections for data-simulation differences.

At present a data sample corresponding to 232 fb^{-1} total integrated luminosity collected by *BABAR* has been analyzed. A total of 4025 events are selected, with an estimated background contamination of about 5% for $m_{p\bar{p}} < 2.5\,\mathrm{GeV}/c^2$, increasing with $m_{p\bar{p}}$ and becoming consistent with 100% above 4.5 GeV/c^2.

The cross section for $e^+e^- \to p\bar{p}$ is calculated from the $p\bar{p}$ mass spectrum as

$$\sigma_{p\bar{p}} \;=\; \frac{dN/dm}{\varepsilon\, R\, dL/dm}, \tag{6}$$

where m is the center value of the $p\bar{p}$ mass bin, dN/dm is the number of signal events selected in that mass bin, corrected for resolution effects, dL/dm is the ISR differential luminosity, ε is the total reconstruction efficiency as a function of mass, and R is a factor taking into account the radiative corrections due to multiple photons emission. The ISR luminosity is calculated from the total integrated luminosity and the radiator function integrated over the angular distribution.

Radiative corrections have been evaluated according to the structure function method, but do not include corrections due to vacuum polarization. Hence what is quoted here is the so called "dressed" cross section. The invariant mass resolution has been unfolded, however the chosen bin widths exceed the resolution. The resulting cross section as a function of the mass of the $p\bar{p}$ system is shown in Fig. 5, statistical and systematic uncertainties included. Results from all the previous experiments are also shown: BES [10], CLEO [11], FENICE [12], DM2 [13], DM1 [14] and ppbar [15].

The *BABAR* data cover the range from threshold up to $4.5\,\mathrm{GeV}/c^2$ and look in agreement with previous results, however, thanks to the smaller errors, unexpected features are now visible: the cross section shows a plateau from threshold up to $\sim 2.1\,\mathrm{GeV}/c^2$, and two drops at $\sim 2.2\,\mathrm{GeV}/c^2$ and $\sim 3\,\mathrm{GeV}/c^2$.

3. Angular distribution and measurement of $|G_E^p/G_M^p|$

The ratio of electric to magnetic form factor can be extracted analyzing the distribution of the proton helicity angle in the $p\bar{p}$ rest frame. In general this distribution can be written as:

$$\frac{dN}{d\cos\theta_p} \;=\; A\left(H_M(\cos\theta_p, m_{p\bar{p}}) + \left|\frac{G_E}{G_M}\right| H_E(\cos\theta_p, m_{p\bar{p}})\right)\;. \tag{7}$$

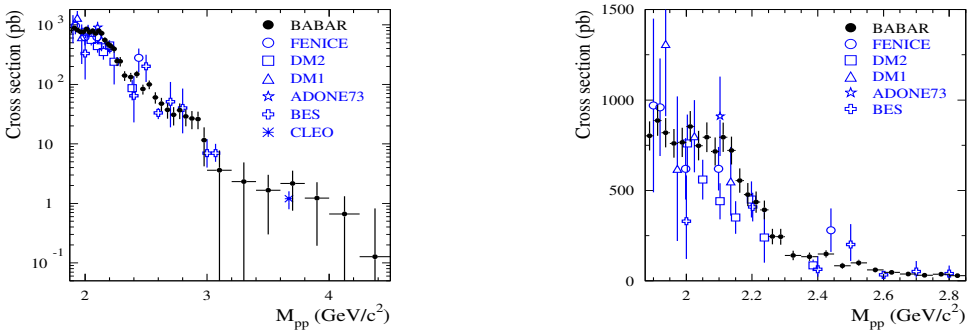

Figure 5. (Left) The $e^+e^- \to p\bar{p}$ cross section measured in *BABAR* compared to previous experiments as a function of the mass of the $p\bar{p}$ system, $m_{p\bar{p}}$. (Right) Detail of the region $m_{p\bar{p}} < 2.9\,\mathrm{GeV}/c^2$ in linear scale.

The functions $H_M(\cos\theta_p, m_{p\bar{p}})$ and $H_E(\cos\theta_p, m_{p\bar{p}})$ do not strongly differ from the functions $\sin^2\theta_p$ and $1+\cos^2\theta_p$, respectively. The exact expressions are obtained via Monte Carlo simulation. The mass region from $p\bar{p}$ threshold up to 3 GeV/c^2 is divided in six intervals. For

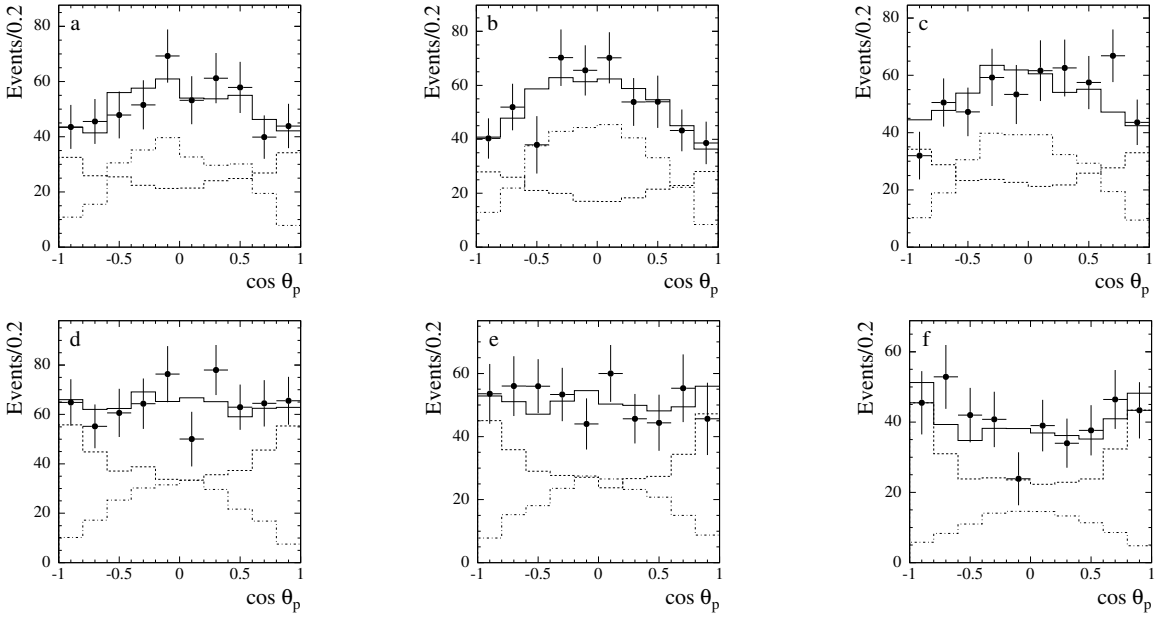

Figure 6. *BABAR* data: distributions of the proton helicity angle in the $p\bar{p}$ rest frame for different invariant mass regions. From plot "a" to "f", the energy regions are respectively 1.877-1.950 GeV/c^2, 1.950-2.025 GeV/c^2, 2.025-2.100 GeV/c^2, 2.100-2.200 GeV/c^2, 2.200-2.400 GeV/$c^2$and 2.400-3.000 GeV/c^2. The points with errors are the background-subtracted data, the solid histogram is the fit result and the dashed and dot-dashed histograms show the separate contributions of the terms corresponding to magnetic and electric form factos, respectively.

each mass bin the angular distribution after background subtraction is shown in Fig. 6. These distributions are fitted by Eq.(7), with two free parameters: A and $|G_E/G_M|$. The functions H_E and H_M are replaced by the histograms obtained from the Monte Carlo simulation. Fig. 6 shows the result of the fits, together with the separate contribution from the two terms.

BABAR measures values of $|G_E/G_M|$ significantly greater than unity, as shown in Fig. 7, in disagreement with previous results from experiment PS170 at LEAR [16]. We should note,

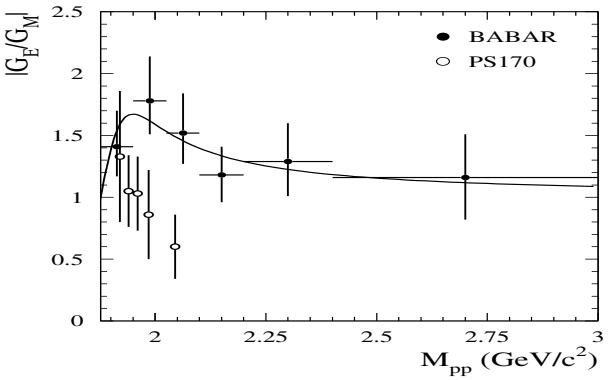

Figure 7. The ratio $|G_E/G_M|$ as a function of the $p\bar{p}$ mass measured by *BABAR* (filled circles) and by PS170 experiment (open circles). The line is the result of the fit to *BABAR* data.

however, that PS170 data were limited by a non complete angular acceptance and were affected by strong angular dependence of the detection efficiency, while one of the advantages of ISR technique over conventional e^+e^- and $p\bar{p}$ experiments is just that the detection efficiency is very weakly dependent on invariant mass and angular distributions.

4. Measurements of $|G_M^p|$

The $e^+e^- \to p\bar{p}$ cross section is a function of two form factors, but due to the poor determination of the $|G_E/G_M|$ ratio, they cannot be extracted from the data simultaneously with reasonable accuracy.

At production threshold $|G_E^p(4m_p^2)| = |G_M^p(4m_p^2)|$, while, at high q^2 the contribution of G_E^p to the cross section becomes negligible, because of the $4m_p^2/q^2$ suppression factor. Therefore, the experiment usually quote measurements of $|G_M^p|$ under the assumption $|G_E^p(q^2)| = |G_M^p(q^2)|$. This assumption is actually true only at production threshold, while it is fully arbitrary for a generic q^2 value, and, as we have just seen, is also in disagreement with the *BABAR* measurement of the $|G_E/G_M|$ ratio. However, also *BABAR* published the proton form factor distribution under this assumption in order to make the results comparable with the previous ones.

4.1. Overview of the experimental situation

The first attempt to measure the proton form factor was performed in 1965 at CERN [17], looking for $p\bar{p}$ annihilation at $\sqrt{s} = m_{p\bar{p}} = 2.61$ GeV/c^2. No events were collected and only an upper limit on the cross section was set. Upper limits were also set at $s = 2.26$ and $s = 2.57$ GeV/c^2, again studying the process $p\bar{p} \to e^+e^-$, at the Brookhaven National Laboratories [18], in 1969.

In 1973 the first succesfull measuremet of the proton form factor was obtained at the e^+e^- ring ADONE in Frascati [15], where 25 $e^+e^- \to p\bar{p}$ events were collected at $s = 2.10$ GeV/c^2, followed two years later by a measurement at $s = 3.10$ GeV/c^2 performed by the experiment DASP [19], with another e^+e^- machine, DORIS at DESY.

Several more measurements have been performed at e^+e^- accumulation rings in the following 30 years. All the experiments were based on the measurement of the $e^+e^- \to p\bar{p}$ cross section for different energies of the colliding beams (see Fig. 5).

Only a limited energy range was available for each machine, so that the experiments DM1 [14] and DM2 [13] at DCI (Orsay), and FENICE at ADONE, could cover approximately the region $1.92 < s < 2.45$ GeV/c^2, while BES [10] at BEPC, covered the range between 2.4 and 3 GeV/c^2.

Moreover, because of the low luminosity of these machines, only few tens of events, if not less, have been collected per point.

As already observed, the cross section at threshold is not accessible at e^+e^- colliders because of the vanishing momenta of the two protons. The measurement at threshold has been instead performed stopping antiprotons in a hydrogen target, first by the ELPAR [20] experiment at the CERN protosincrotron, and later by the PS170 [21] at LEAR. PS170 collected about 3700 events measuring very precisely the form factor in the region close to the threshold [22]. The large geometrical acceptance, as discussed before, allowed the measurement of the angular distribution of the produced electrons and to extract the $|G_E/G_M|$ ratio.

The region at high momentum transfer has been measured in the last 15 years by a series of $p\bar{p}$ experiments mainly dedicated to charm spectroscopy, installed on the antiproton accumulator at Fermilab, namely E760 [23] and E835 [24, 25]. Globally, these experiments were able to measure about 10 points in the range $2.96 < s < 3.8$ GeV$/c^2$.

All measurements are shown in Fig. 8, together with those presented by *BABAR*, whose $\sim$ 4000 events ranging from threshold up to 4.5 GeV$/c^2$, have been divided in 40 energy bins.

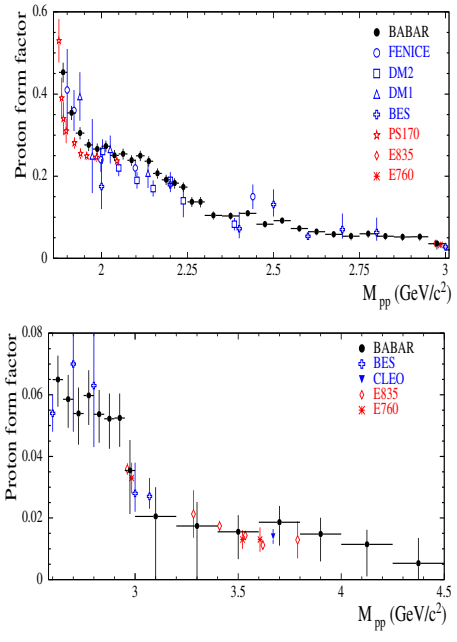

Figure 8. $|G_M^p|$ as a function of the mass of the $p\bar{p}$ system, according to the existing measurements performed in e^+e^- and $p\bar{p}$ experimental facilities. Note the different vertical scale between the left plot ($m_{p\bar{p}} < 3\text{GeV}/c^2$) and the right plot ($3 < m_{p\bar{p}} < 4.5\text{GeV}/c^2$).

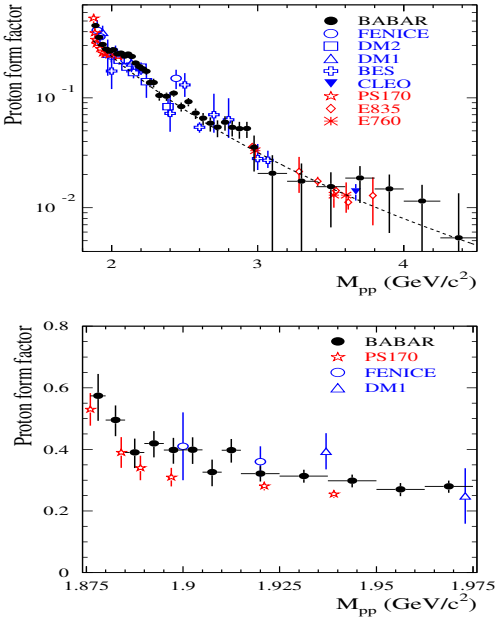

Figure 9. (Top) fit to the perturbative QCD prediction using all proton form factor data; (bottom) the proton form factor near $p\bar{p}$ threshold.

4.2. Fit to perturbative QCD prediction

The perturtbative QCD ($pQCD$) predicts for the magnetic proton form factor the asymptotic behavior [26]

$$G_M(Q^2) = \frac{32\pi^2}{9} C \frac{\alpha_s^2(Q^2)}{Q^4} \left(ln \frac{Q^2}{\Lambda^2} \right)^{-\frac{4}{27}}; \qquad (8)$$

where $\alpha_s \sim \left(ln\frac{Q^2}{\Lambda^2}\right)^{-1}$ is the strong coupling constant, Λ is the QCD mass scale, and C is a costant parameter which has to be determined by the experimental results. Fig. 9(top) shows the result of the fit to all existing data with $m_{p\bar{p}} > 3\,\mathrm{GeV}/c^2$, assuming $\Lambda = 0.3\,\mathrm{GeV}$. It is seen that the asymptotic regime is indeed reached quite early.

However, the fit curve is about a factor two higher than the corresponding curve in the space-like region, while according to the Phragmèn-Lindelöff theorem for analytical functions as the form factors, space-like and time-like asymptotic behavior must be, in modulus, the same [27].

4.3. Shape of the FF distribution

The rapid decreases of the form factor observed at the same energies as for the cross section, that is near $2.2\,\mathrm{GeV}/c^2$ and $3\,\mathrm{GeV}/c^2$, are of difficult interpretation and have not yet been discussed in the literature.

The distribution presents also a very steep behavior near threshold. This feature was first observed by PS170 and is now confirmed by the *BABAR* data, as can be better seen on the bottom of Fig. 9 where the form factor has been calculated over a smaller bin width, to account for the rapid change of his value with $m_{p\bar{p}}$ in this region. A similar behavior has been observed also in the mass distribution of the $p\bar{p}$ system produced in different processes, characterized by different dynamics and in some cases also by different quantum numbers. This is the case for example for the $p\bar{p}$ mass spectrum observed in B decays like $B^0 \to D^{(*)}p\bar{p}$ and $B^+ \to K^+p\bar{p}$, both by Belle [28] and *BABAR*. Interesting are also the radiative $J/\psi \to \gamma p\bar{p}$ decays measured by BES [29]. In this case the $p\bar{p}$ system has positive charge parity and its mass spectrum shows a sharp peak at threshold, which has been fit with a Breit-Wigner resonance function. The fit results incompatible with all the known states, while it is consistent with the presence of a new pseudoscalar resonant structure at a mass of $\simeq 1.860\,\mathrm{GeV}/c^2$, below the $p\bar{p}$ threshold, and a width $\Gamma < 30$ MeV at the 90% *C.L.*

This state could be related to a state with similar mass and width, but opposite charge parity, $J^{PC} = 1^{--}$, which could produce the enhancement at threshold of the magnetic form factor. A state with such characteristics is indeed suggested by the result of a fit to the experimental data (*BABAR* and last BES data were not yet available) by means of dispersion relations in the unphysical region [30].

The presence of a narrow $N\bar{N}$ bound state below threshold, should show up as a dip in $e^+e^- \to hadrons$ cross sections, as a consequence of interference with a broad resonance [31]. Such an effect has been clearly seen in 6π production by DM2, in $e^+e^- \to 3(\pi^+\pi^-)$ reactions, and by E687 experiment in photo-production of the $3(\pi^+\pi^-)$ final state [32]. Both experiments fit a mass $m \simeq 1.9$ GeV/c^2 and a width $\Gamma \simeq 35\,\mathrm{MeV}$.

BABAR observe a dip both in $e^+e^- \to 3(\pi^+\pi^-)$ and $e^+e^- \to 2(\pi^+\pi^-\pi^0)$ [33] channels. The fit masses are similar to those found by DM2 and E687, while the widths are significantly larger ($\sim 150\,\mathrm{MeV}$).

5. Neutron time-like form factor

The magnetic neutron form factor is shown in Fig. 10(left), as achieved by FENICE and DM2. FENICE [12] collected an integrated luminosity of ~ 500 nb^{-1} in the CM energy range $1.9 < s < 2.55\,\mathrm{GeV}$, while DM2 results were based only on few candidate events.

FENICE measured both $e^+e^- \to n\bar{n}$ and $e^+e^- \to p\bar{p}$ cross section finding

$$R_N = \frac{\sigma(e^+e^- \to p\bar{p})}{\sigma(e^+e^- \to n\bar{n})} \sim 2, \tag{9}$$

as shown in Fig. 10(right). Assuming a leading quark in the nucleon, $R_N \sim (Q_d/Q_u)^2 = 0.25$ is

naively expected. Similar results are obtained by calculation based on dispersion relations and pQCD asymptotic behavior.

These contradicting results suggest that the measurement of $e^+e^- \to n\bar{n}$ should be redone with much higher statistics, in particular in the near threshold region.

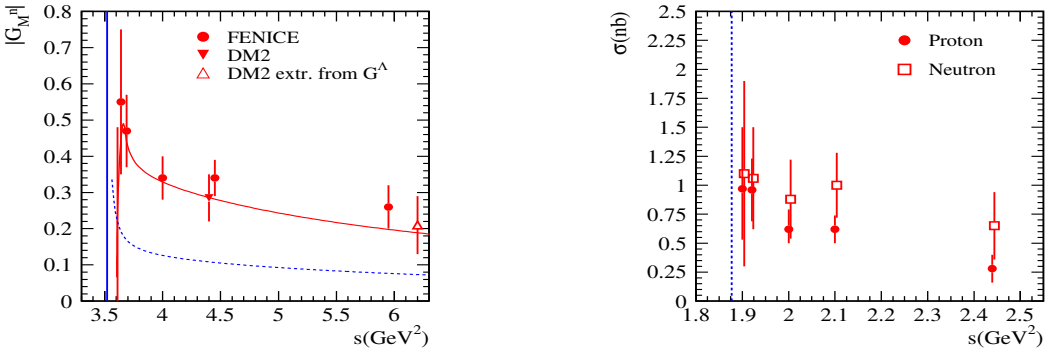

Figure 10. (Left) The neutron form factor as measured by FENICE and DM2; the dashed line is the proton form factor scaled by the d and u quarks charge ratio: $|G_M^p\, Q_d/Q_u|$. (Right) The $p\bar{p}$ and $n\bar{n}$ cross sections measured by FENICE.

6. Conclusions and perspectives

The proton form factors in the time-like region have been measured for the last thirty years both at e^+e^- and $p\bar{p}$ facilities. Recently *BABAR* measured with very good accuracy the $e^+e^- \to p\bar{p}$ cross section and the magnetic form factor from threshold up to $\sim 4.5\,\mathrm{GeV}$. by means of the ISR processes. However, several unexplained effects are yet to be fully understood, namely:

- the asymptotic behavior of the magnetic form factor seems to agree with perturbative QCD expectetions already at $q^2 \sim 9\mathrm{GeV}^2$, but it is about a factor of two higher than the corresponding fit in the space-like region, while QCD and analyticity predict $|G_M(q^2)| = |G_M(-q^2)|$;
- unexplained drops are observed both in the cross section and in form factor distribution;
- the magnetic form factor exhibits a sharp enhancement at threshold, as observed by PS170 and confirmed by *BABAR*; this behavior could be related to similar enhancememnts observed in the mass of the $p\bar{p}$ system in several decays and to the dips observed in productions of multi-hadrons states;
- *BABAR* measured a $|G_E/G_M|$ ratio significantly greater than unity after threshold in clear disagreement with previous PS170 results;
- the $e^+e^- \to p\bar{p}$ cross section looks smaller by a factor two than the $e^+e^- \to n\bar{n}$ one, contrary to what expected according to QCD.

These open issues would greatly benefit of new more precise measurements. No dedicated experiments are presently planned, but the nucleon structure can be studied at several operating or planned facilities.

Let me mention that by the end of the run in 2008, *BABAR* should have collected four times the statistics used for the published analysis, and similar results are expected very soon from Belle.

Also BES-II, which should start taking data at the tau-charm factory BEPC next year, can use the same technique based on ISR to measure $e^+e^- \to p\bar{p}$ with very high accuracy, while the

e^+e^- collider in Novosibirsk, VEPP2M, should perform an energy scan in the near threshold region.

Moving to a farther future, the PANDA experiment plans to measure the $p\bar{p} \to e^+e^-$ cross section up to $m_{p\bar{p}} \sim 5$ GeV/c^2.

A proposal has been presented in Frascati to repeat the FENICE measurements on both $e^+e^- \to p\bar{p}$ and $e^+e^- \to n\bar{n}$ reactions at a new high luminosity e^+e^- collider.

Finally, the *BABAR* measurements could be repeated with two-three order of magnitudes more data at a super-B factory capable to reach a luminosity of $\sim 10^{36}\,\mathrm{cm}^{-2}\mathrm{s}^{-1}$.

Acknowledgments

I am thankful to my colleagues from the *BABAR* Collaboration for providing material for the talk, with special thanks to R. Baldini, S. Pacetti, A. Zallo, E. Solodov and V. Druzhinin for the useful discussions. I wish also to thank the organizers of the *2nd Meeting of the APS Topical Group on Hadron Phyisics* for their kind hospitality.

[1] Jones M K *et al*, *Phys. Rev. Lett.* **84**, 1398 (2000); Gayou O *et al*, *Phys. Rev. Lett.* **88**, 092301 (2002)
[2] Landau L D and Lifshitz E M 1981 *Quantum Mechanics*, (Butterworth-Heinemann)
[3] Arbuzov A B*et al*, *JHEP* **9812**, 009 (1998); Binner S, Kuhn J H and Melnikov K, *Phys. Lett.* B **459**, 279 (1999); Benayoun M *et al*, *Mod. Phys. Lett.* A **14**, 2605 (1999)
[4] Aubert B *et al*, *Phys. Rev.* D **73**, 012005 (2006)
[5] Aubert B *et al*, *BABAR* Collaboration, *Nucl. Instrum. Methods* A **479**, 1 (2002)
[6] Czyz H and Kuhn J H, *Eur. Phys. J.* C **18**, 497 (2001)
[7] Arbuzov A B *et al*, *JHEP* **9710**, 001 (1997)
[8] Caffo M, Czyz H and Remiddi E, *Nuovo Cimento* **A110**, 515 (1997); *Phys. Lett.* B **327**, 369 (1994)
[9] Barberio E, van Eijk B and Was Z, *Comput. Phys. Commun.* **66**, 115 (1991)
[10] Ablikim M *et al*, BES Collaboration, *Phys. Lett.* B **630**, 14 (2005)
[11] Pedlar T K *et al*, CLEO Collaboration, *Phys. Rev. Lett.* **95**, 261803 (2005)
[12] Antonelli A *et al*, FENICE Collaboration, *Nucl. Phys.* B **517**, 3 (1998)
[13] Bisello D*et al*, DM2 Collaboration, *Nucl. Phys.* B **224**, 379 (1983); *Z. Phys.* C **48**, 23 (1990)
[14] Delcourt B *et al*, DM1 Collaboration, *Phys. Lett.* B **86**, 395 (1979)
[15] Castellano D *et al*, ppbar Experiment, *Nuovo Cimento* **14**, 1 (1973)
[16] Bardin G *et al*, PS170 Collaboration, *Nucl. Phys.* B **411**, 3 (1994)
[17] Conversi M *et al*, *Nuovo Cimento* **40**, 690-701 1965
[18] Hartill D L *et al*, *Phys. Rev.* 184, 1415, (1969)
[19] Braunschweig W *et al*, *Phys. Lett.* B **57**, 297 (1975)
[20] Bassompierre G *et al*, *Phys. Lett.* B **68**, 477 (1976)
[21] Bardin G *et al*, PS170 Collaboration, *Phys. Lett.* B **255**, 149 (1991)
[22] Bardin G *et al*, PS170 Collaboration, *Phys. Lett.* B **257**, 514 (1991)
[23] Armstrong T A *et al*, E760 Collaboration, *Phys. Rev. Lett.* **70**, 1212 (1993)
[24] Ambrogiani M *et al*, E835 Collaboration, *Phys. Rev.* D **60**, 032002 (1999)
[25] Andreotti M *et al*, E835 Collaboration, *Phys. Lett.* B **559**, 20 (2003)
[26] Lepage G and Brodsky S, *Phys. Rev.* D **22**, 2157 (1980) and references therein
[27] Tichmarsch E C 1939 *The theory of functions*, (London: Oxford University Press)
[28] Abe K *et al*, Belle Collaboration, *Phys. Rev. Lett.* **88**, 181803 (2002); *Phys. Rev. Lett.* **89**, 151802 (2002);
[29] Bai J Z *et al*, BES Collaboration, *Phys. Rev. Lett.* **91**, 022001 (2003);
[30] Baldini R *et al*, *Eur. Phys. J.* C **11**, 709 (1999)
[31] Franzini P J and Gilman F J, *Phys. Rev.* D **32**, 237 (1985)
[32] Frabetti P L *et al*, E687 Collaboration, *Phys. Lett.* B **514**, 240 (2001)
[33] Aubert B *et al*, *BABAR* Collaboration, *Phys. Rev.* D **73**, 052003 (2006)